Melting the Ice: On the Relation between Melting Temperature and Size for Nanoscale Ice Crystals

Ding Pan,[†,∥] Li-Min Liu,[‡] Ben Slater,[§] Angelos Michaelides,[‡,§,*] and Enge Wang[⊥]

[†]Institute of Physics, Chinese Academy of Sciences, P.O. Box 603, Beijing 100190, People's Republic of China, [‡]London Centre for Nanotechnology, University College London, London WC1H 0AJ, U.K., [§]Department of Chemistry, University College London, London WC1H 0AJ, U.K., and [⊥]School of Physics, Peking University, Beijing 100871, People's Republic of China. [∥]Present address: Department of Chemistry, UC Davis, California, United States

ABSTRACT Although the melting of ice is an everyday process, important issues remain unclear particularly on the nanoscale. Indeed despite extensive studies into ice melting and premelting, little is known about the relationship between (pre)melting and crystal size and morphology, with, for example, the melting temperature of ice nanocrystals being unclear. Here we report extensive long-time force-field-based molecular dynamics studies of the melting of hexagonal ice nanocrystals in the *ca.* 2 to 8 nm size range. We show that premelting is initiated at the corners of the crystals, then the edges between facets, and then the flat surfaces; that is, the melting temperature is related to the degree of coordination. A strong size dependence of the melting temperature is observed, with the combination of small particle size and premelting leading nanosized ice crystals to have liquid-like surfaces as low as about 130 K below the bulk ice melting temperature. These results will be of relevance in understanding the size dependence of ice crystal morphology and the surface reactivity of ice particles under atmospheric conditions.

KEYWORDS: ice · water · nanocrystal · molecular dynamics · melting · premelting · finite size effects

The melting of ice is a very familiar process, but its ubiquity belies its importance. It plays a central role in a wide variety of chemical processes and is particularly relevant to environmental and atmospheric chemistry. It has been anticipated since the time of Faraday that at temperatures below zero degrees Celsius a liquid film of water forms on the ice surface.[1] However, some 160 years or so later this "premelting" or "quasi-liquid" layer remains a matter of debate and has been the subject of numerous recent experimental and theoretical studies (see, for example, refs 2−19). Much of this work has focused on understanding the surfaces of bulk (macroscopic) ice crystals and usually with an emphasis on the basal surface. Much less attention, however, has been paid to the melting and premelting behavior of smaller ice particles, such as those in the nanometer size range. It is important to understand such particles not least because they occur in polar mesospheric clouds, which occur at altitudes of about 80−90 km and are sometimes known as noctilucent clouds because of how light is scattered from the water/ice nanoparticles they contain.[20] In particular, questions related to the structure and properties at temperatures relevant to noctilucent clouds (*ca.* 120 K) remain unresolved.

In the laboratory it is difficult to prepare isolated nanosized ice clusters.[21] Often they are grown on a substrate, such as in surface-science style studies of ice nanoclusters supported on metal surfaces (see for example, refs 22−24). So far studies of such metal-supported clusters have focused on characterizing the structures of the clusters and in exploring how they diffuse across the surface. Melting temperatures have not yet been determined. However, given the strong interaction that is present between these clusters and the substrate, they cannot be expected to display melting properties characteristic of isolated crystals. In contrast to experiment, with computer simulation techniques it is relatively straightforward to explore isolated crystals. For example, Egorov *et al.*[25] used empirical potentials to examine how the melting point changed with cluster size for some very small (from 8 to 40 molecule) water clusters. A nonmonotonic decrease in melting temperature was observed upon going to progressively smaller clusters, behavior that is likely attributed to the very small cluster sizes examined. Similarly, Pereyra and Carignano[26] studied the melting of ice nanocolumns, whose initial cross section was rectangular. This study was a particularly valuable contribution, as the dependence of the melting point depression on the width of the nanocolumns was explored, and clear finite size effects were observed. Despite this recent progress, there are a number of interesting and important questions related

* Address correspondence to angelos.michaelides@ucl.ac.uk.

Received for review January 20, 2011 and accepted May 13, 2011.

Published online May 13, 2011
10.1021/nn200252w

to ice nanocrystal melting that have still not been tackled. In this work, we have focused on the following questions: (i) How does the melting and premelting temperature change with crystal size across the nanometer size regime? (ii) How does the morphology of the ice crystals change as they melt? (iii) Where on the nanocrystals is the melting initiated, and how does the melting differ at different locations of the crystals (flat surfaces, edges, corners)? To answer these questions, we have performed long molecular dynamics simulations with the TIP4P force field on hexagonal ice nanocrystals in the *ca.* 2 to 8 nm size regime. We have examined hexagonal platelet structures, as these are often observed under natural and experimental conditions and expose both prism and basal surfaces as well as edges and corners. The underlying crystal structure of the ice particles is hexagonal ice Ih, the most common form of ice, although we note that on the nanoscale crystals of ice Ic have also been observed.[27]

The main results to come from this study are that premelting is initiated at the corners of the crystals, then the edges between facets, and then the flat surfaces. A strong size dependence of the melting temperature is observed, with the combination of small particle size and premelting leading nanosized ice crystals to have liquid-like surfaces as low as about 130 K below the bulk ice melting temperature. We show, however, that this size dependence follows the classical Gibbs–Thomson relation reasonably well. We believe that these results will be of relevance in understanding the size dependence of ice crystal morphology and the surface reactivity of ice particles under atmospheric conditions, specifically conditions relevant to polar mesospheric clouds.

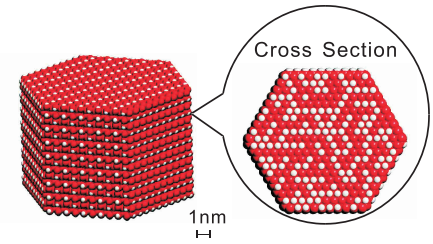

Figure 1. Hexagonal ice nanocrystal before premelting, with ordered proton arrangements at each surface. A (0001) cross section shows that in the interior of the crystal the protons are disordered (see methods). Red balls are oxygen atoms and white ones are hydrogen atoms, both of which are increased in size in order to show the proton distributions more clearly.

RESULTS AND DISCUSSION

Nanocrystal Melting Temperatures. A series of molecular dynamics simulations using the TIP4P force field was performed on the melting of ice nanocrystals in the *ca.* 2 to 8 nm size regime. The number of water molecules in the clusters varied from 768 to 9600, and the structure of a typical nanocrystal considered is shown in Figure 1. Further details of the computational setup, ice crystal structures, information and justification of the potential model used, and protocol used to determine accurate melting temperatures are given in the Methods section.

In the beginning we want to obtain a general picture of how the ice nanocrystals melt. In Figure 2 we show snapshots from our MD simulations of two ice nanocrystals with 9600 and 2592 water molecules at four different temperatures. It is clear that as the temperature increases the order within the nanocrystals diminishes and the overall shapes of the crystals change from hexagonal to spherical. The water molecules in the core of the ice nanocrystals maintain their ordered hexagonal arrangement right up until about 5 to 2.5 K below the melting points. At the surface the disorder (premelting) sets in at much lower temperatures and is already apparent from the images in Figure 2 some 30 to 40 K below the melting point. These qualitative features are common for all the ice nanocrystals investigated here.

The snapshots in Figure 2 give an indication of when the crystals melt, but in order to establish the melting temperatures more precisely, we look at how

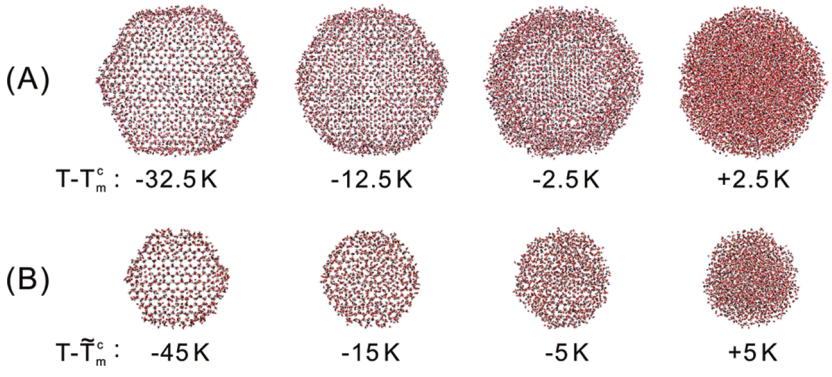

Figure 2. Snapshots of the ice nanocrystals with (A) 9600 water molecules and (B) 2592 water molecules. The temperature below each ice nanocrystal, ΔT, is the difference between the simulation temperature T and the melting temperature T_m^c; $\Delta T = T - T_m^c$. T_m^c = 212.5 K for the 9600 water molecule cluster and $\tilde{T}_m^c$ = 195.5 K for the 2592 water molecule cluster.

the potential energy changes with temperature. The variation in potential energy with temperature is shown in Figure 3 for all nanocrystals considered. In general we see that the potential energy increases gradually with temperature up until the melting point of the nanocrystals, T_m^c, at which point it increases abruptly, at the first-order transition point. For the ice nanocrystals with 9600 water molecules, the jump in the potential energy is between 210 and 215 K, so we estimate T_m^c to be about 212.5 ± 2.5 K (the bulk melting temperature for this TIP4P model is T_m^b = 230 ± 3 K).[17] The melting temperature for the ice nanocrystal with 6144 water molecules is estimated to be 207.5 ± 2.5 K. For the one with 2592 water molecules it is T_m^c = 195.0 ± 5.0 K, and for the 768-molecule nanocrystal it is T_m^c = 175.0 ± 5.0 K. In addition to simply examining the nanocrystals and evaluating changes in potential energy, we also monitored the diffusion coefficients of the molecules within the nanocrystals, which is another good way to judge when the crystals melt. The melting temperatures obtained from analysis of the diffusion coefficients agree with those obtained from the potential curves (and by simply looking at the nanocrystals). Thus we have three separate measures of the melting temperatures, and together with the care taken to ensure that sufficiently long MD simulations were performed we have confidence in our melting temperature determinations.

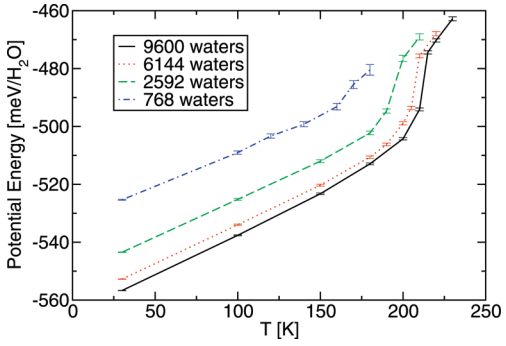

Figure 3. Potential energy changes with temperature for the ice nanocrystals with 768, 2592, 6144, and 9600 water molecules. The estimated error bar on each data point is also indicated.

Clearly a large variation in melting temperature with nanocrystal size is observed, with T_m^c decreasing as the cluster size decreases (Figure 4A). Such melting point depressions are common for nanoscale materials and can sometimes be described by the Gibbs–Thomson relation.[28] However, the validity of the Gibbs–Thomson relation for ice nanoparticles is unclear,[29–31] and for certain materials (*e.g.*, metal nanoclusters[32]) significant deviations are observed on the nanoscale. Given our evaluations of T_m^c for a range of nanocrystals, we are now in a position to assess the validity of the Gibbs–Thomas relation for water–ice on the nanoscale. The Gibbs–Thomson relation predicts a melting point depression as follows:

$$\Delta T_m^c = T_m^b - T_m^c = \frac{\gamma T_m^b K}{L} \quad (1)$$

where $\Delta T_m^c = T_m^b - T_m^c$ is the difference between the bulk melting temperature T_m^b and the actual nanocrystal melting temperature T_m^c, γ is the solid/liquid interface energy, L is the volumetric latent heat of melting, and K is the mean curvature of the solid/liquid surface. $K = dA/dV$, where A is the surface area and V is the volume. Values for the parameters, T_m^b and L in eq 1 were taken from previous work.[33] With the help of a fitted water/ice interface energy γ of 46.7 mJ/m^2, the predicted Gibbs–Thomson line is shown in Figure 4B. Also plotted in Figure 4B are the melting temperatures established from the MD simulations. It is clear that for the range of nanocrystals explored the melting temperatures obtained from the simulations and predicted by the Gibbs–Thomson relation agree very well.[34] This demonstration that ice nanocrystal melting temperatures follow the Gibbs–Thomson relation is of value, as it enables useful predictions to be made for ice crystal melting temperatures of arbitrary size. This is important to, for example, researchers in the atmospheric sciences community who are interested in

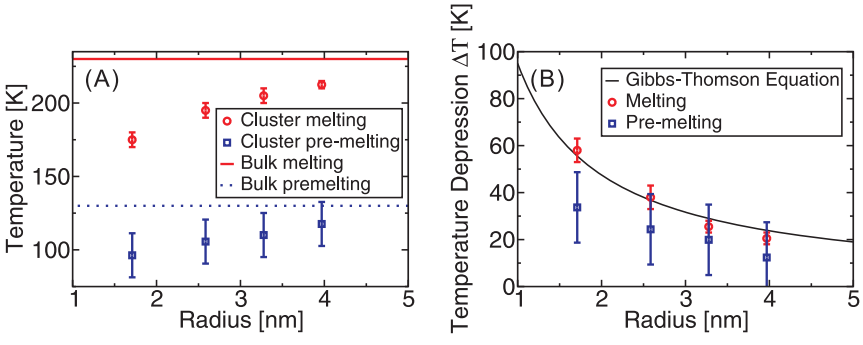

Figure 4. (A) Variation of the melting and premelting temperature with nanocrystal size obtained from the MD simulations. The red solid and blue dotted lines show the bulk melting temperature and premelting temperature, respectively. (B) Temperature depression with nanocrystal size and the Gibbs–Thomson relation (black line). The melting point depression is defined as $\Delta T_m^c = T_m^b - T_m^c$, and the premelting temperature depression as $\Delta T_{pm}^c = T_{pm}^b - T_{pm}^c$. The estimated error bar on each data point is also indicated.

understanding the properties and reactivity of ice particles in the mesosphere. We note that in a recent study by Pereyra and Carignano,[26] in which infinitely long nanoclumns were explored, the melting temperature of the nanoclumn was shown to vary with its diameter in an analogous manner to what is observed here. However, the extent of the melting point depression was somewhat smaller than in the present study. This is most likely due to the different ice crystal morphologies considered in the two studies, and in particular to the absence of corner sites in the infinitely long nanocolumns. In a more general sense it is interesting to note that ice as a hydrogen-bonded nanocrystal follows the classical Gibbs–Thomson equation, whereas other materials such as metal[32] and semiconductor[35] nanoparticles exhibit more dramatic variations in melting temperatures with crystal size.

Nanocrystal Premelting Temperatures. As discussed, the ice nanocrystals examined here exhibit a premelting layer before the onset of bulk melting. The presence of premelting layers on ice surfaces in general is now well-established (for example, refs 2–18). However, the sensitivity of the premelting layer to nanocrystal size is unclear.[36,37] Using our MD simulations we can directly assess the crystal size dependence on the premelting layer, which is what we discuss in the following.

We begin, however, by defining more precisely what we mean by the liquid layer and some other related quantities. Following Conde *et al.*,[17] water molecules are classified as being either ice-like or liquid-like with the tetrahedral index

$$q_i = \left[1 - \frac{3}{8}\sum_{j=1}^{3}\sum_{k=j+1}^{4}\left(\cos(\Theta_{j,i,k}) + \frac{1}{3}\right)^2\right] \quad (2)$$

where i, j, and k are indices for the water molecules (or O atoms). The angle $\Theta_{j,i,k}$ is formed by two of the four nearest neighbor O atoms of the ith O atom, j and k, so there are six terms in the sum. For a perfect tetrahedral structure, *i.e.*, $\Theta_{j,i,k}$ of 109°28′, q_i has a value of 1. As q_i approaches 1, the molecules are in a more tetrahedral environment. So the tetrahedral index is a useful tool to distinguish ice-like and non-ice-like structures. Again following Conde *et al.*, when $q_i \geq 0.91$, a molecule is defined as being ice-like; otherwise it is a liquid-like molecule.

The thickness of the quasi-liquid layer is calculated as

$$d_{\text{apparent}} = \frac{n_{\text{quasi-liquid}} M_{H_2O}}{2\rho N_A \pi r^2} \quad (3)$$

where $n_{\text{quasi-liquid}}$ is the average number of quasi-liquid water molecules within a cylinder of radius $r = 0.6$ nm, M_{H_2O} is the molar mass of water, N_A is Avogadro's constant, and ρ is the density of TIP4P water at the melting point, 0.99 g/cm^3.[17] Here, we examine the thickness within an ice cylinder that runs through the ice crystal from one basal plane to the other, and the radius of 0.6 nm is selected so that effects from the edges or corners are eliminated for all nanocrystals (see Figure 5B). We define the onset of premelting as the temperature at which the quasi-liquid layer becomes 0.1 nm thick on the basal plane.[17] With this definition the onset of bulk premelting occurs at about 100 K below the bulk melting temperature. For the nanocrystals, within the error bars of the temperature estimates,[38] the onset of premelting is slightly slower, occurring at about 90 to 95 K below the melting temperature of each nanocrystal, as can be seen in Figure 4A. Hence overall we see that as the size of the nanocrystals decreases, the melting temperature decreases and so too the premelting

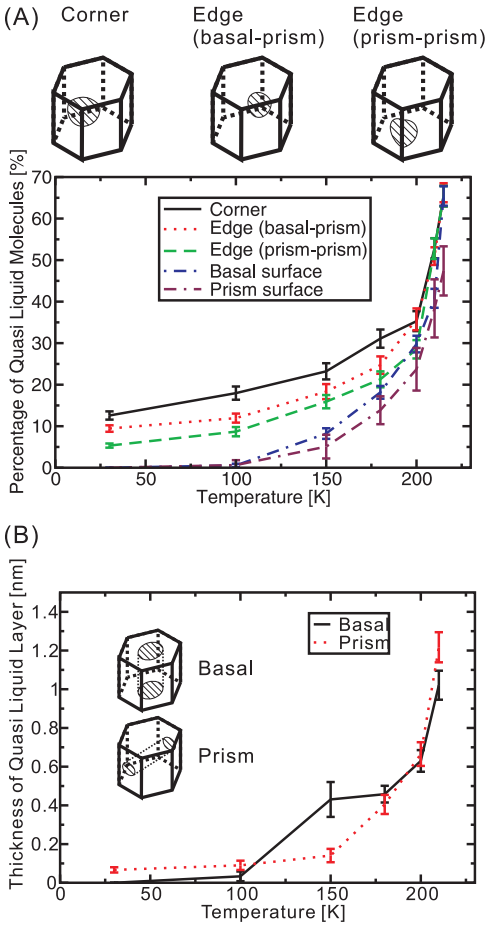

Figure 5. (A) Percentage of quasi-liquid molecules in various regions of the 9600 water molecule nanocrystal as a function of temperature. The regions identified are the corners (solid line), basal–prism edges (dotted line), prism–prism edges (dashed line), and basal and prism surfaces. A sphere with a certain radius is set to intersect with the hexagonal ice nanocrystal to define the corner and edge. The center of the sphere is located at the vertex for the corner, on the sides for the edges, and on the outermost surfaces for the basal and prism faces. (B) Thicknesses of the quasi-liquid layers on the basal (solid line) and prism (dotted line) surfaces of the ice nanocrystal with 9600 water molecules. The average thickness of the quasi-liquid layer in the cylindrical ice core sample (shaded lines) is measured as the premelting thickness. The estimated error bar on each data point is also indicated.

temperature, and as a result, the dependence of premelting temperature on nanocrystal size also follows a trend similar to that predicted by the Gibbs–Thomson relation.

Sensitivity of Melting to Nanocrystal Corners, Edges, and Surfaces. After discussing the size effects of melting and premelting in general, now we look at some specific locations on the hexagonal ice nanocrystal and ask which parts of it will melt first. To this end we look separately at the different corners, edges, and faces. A "corner" is defined as the region where three surfaces intersect and an "edge" where two surfaces intersect. On the particular crystals examined here there are two types of edges, one where two prism surfaces meet at an angle of 120° and one where a prism and a basal surface meet at an angle of 90°. The percentages of the quasi-liquid molecules at the different locations of the 9600-molecule nanocrystal are shown in Figure 5A. In practice, we set a spherical range with a radius of 2.0 nm to classify water molecules in the corners, on the edges, or on the surfaces (on the prism surface, the radius is 1.0 nm). The centers of the spheres are located on the outermost surfaces of the ice nanocrystal (see Figure 5A). Of course, this definition is to some extent arbitrary; however it does provide some useful insight. There are N_{total} water molecules in this spherical range and $n_{quasi\text{-}liquid}$ quasi-liquid molecules. For all temperatures where the basic hexagonal shape persists, the percentages of the quasi-liquid molecules, $n_{quasi\text{-}liquid}/N_{total} \times 100\%$, decreases as we go from the corners, to the basal–prism edges, to the prism–prism edges (Figure 5A). Therefore, this suggests that the "sharper" regions of the nanocrystal have larger fractions of quasi-liquid molecules and that these are the regions that will melt faster. According to the Gibbs–Thomson equation, the melting point depression is proportional to the curvature of an object, which is consistent with the sharper parts of the nanocrystal melting first.

As shown in Figure 5A, the percentages of the quasi-liquid molecules on the basal and prism surfaces are similar. Conde *et al.*[17] reported that for an ice slab the quasi-liquid layer was thicker on the basal surface than on the prism surface. Here, however, we do not see any major differences between the basal and prism faces, except at around 150 K, where the quasi-liquid layer was found to be about 0.2 nm thicker on the basal plane, in accordance with previous findings (Figure 5B).[39]

CONCLUSION

In conclusion, we have performed the first systematic simulation study of the melting of a series of hexagonal ice nanocrystals. Whereas considerable attention has been paid from both experiment and theory to the melting of ice, a detailed study addressing the molecular scale details of ice nanocrystal melting in this size regime has not previously been performed. The nanocrystals examined here are of most relevance to environmental chemistry, where the surfaces of ice particles are known to act as reactive (catalytic) substrates for important chemical processes of relevance to, for example, the properties of polar mesospheric clouds.[20] Here we have shown that the ice nanoparticles experience strong melting point depressions and that along with premelting the ice particles considered can have liquid water covered surfaces as low as about 130 K below the bulk ice melting temperature. This, of course, will have consequences for the chemical reactivity of the ice nanoparticles with liquid-covered particles more prone to the uptake of dissolved gases, especially dissolved salts which have vastly different solubilities in water and ice. In addition, the results reported here may have important consequences for understanding meteoric iron and its removal in polar mesospheric clouds.[40] Experiments have shown that the efficiency of Fe uptake depends strongly on temperature in the 80–150 K temperature range,[41] which may be connected with the appearance of a quasi-liquid layer in small ice nanoparticles as we predict here.

We have also shown that right down to the smallest nanocrystal examined the melting point depression follows the well-known Gibbs–Thomson relation. This is useful since it now allows for simple estimates to be made for the melting temperatures of arbitrary sized ice nanoparticles.

Most prior work on ice melting and ice premelting has focused on understanding the surfaces of macroscopic ice crystals, usually with an emphasis on the basal surface. Our studies here on the hexagonal ice nanoclusters are of interest because the nanoparticles expose basal and prism faces as well as edge and corner sites. This has allowed us to precisely explore how the propensity for premelting depends on local geometry. We find, as could easily have been anticipated, that the premelting is initiated at the corner sites of the nanocrystals. This is then followed by melting at the basal–prism edges, then the prism–prism edges, and then the basal and prism faces. Such inhomogeneities in melting is something that could be explored with, for example, scanning probe techniques for supported ice particles, and we hope this work will prompt such follow-up studies.

METHODS

Since the aim of this study was to explore the melting of isolated ice crystals in the nanometer size range, we employed force-field-based MD approaches. Both the large crystal size and long time-scale simulations required to establish accurate melting temperatures (see below) make a first-principles based study of ice nanocrystal melting unfeasible at present. The high

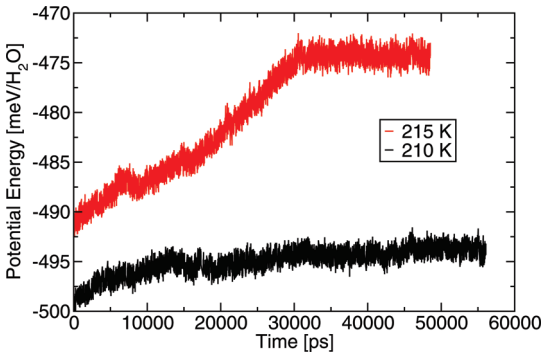

Figure 6. Variation in the potential energy of a 9600 water molecule ice nanocrystal with MD simulation time at 210 K (before total melting) and 215 K (after total melting). The melting temperature for this nanocrystal is $T_m^c = 212.5 \pm 2.5$ K with the TIP4P potential.

melting temperatures (>400 K) predicted by widely used density functional theory (DFT) exchange correlation functionals such as Perdew–Burke–Ernzerhof (PBE)[42] and Becke–Lee–Yang–Parr (BLYP)[43–45] are a further reason to favor force fields over DFT.[46] In this study we opted for the TIP4P[47] model, which has been widely used to treat water and ice and describes many features of the water phase diagram with impressive precision.[48] In addition, the TIP4P model can maintain stable hexagonal ice structures and ice/water interfaces.[11,49] The melting point for TIP4P bulk ice is $T_m^b = 230 \pm 3$ K,[17] and throughout this article we generally discuss melting and premelting temperatures relative to this bulk value, $\Delta T = T - T_m^b$. Although the predicted melting temperature is underestimated, TIP4P is believed to capture the correct structural behavior in the premelting regime. Indeed, recently it was shown for a range of nonpolarizable empirical potentials, *e.g.*, TIP4P/ICE,[50] TIP4P/2005,[51] TIP4P, and SPC/E,[52] that the thickness of the quasi-liquid layer at a given ΔT was insensitive to the potential used.[17]

MD simulations have been performed with the Gromacs simulation package, v.3.3.3,[53] in the canonical (*i.e.*, NVT) ensemble. A 1 fs time step is used throughout, and a Nosé-Hoover thermostat with a relaxation time of 1 ps[54,55] is used to control temperature. The van der Waals interaction is modeled using a Lennard-Jones potential truncated at 1.20 nm, but no cutoff procedure is performed in calculating the Coulomb forces. For the larger nanocrystals (containing 9600, 6144, and 2592 molecules) an Ewald sum was used to treat the Coulomb potential, whose real part has a radius of 0.9 nm. The long-ranged part is calculated in Fourier space by Essmann's particle mesh Ewald (PME) method.[56] The maximum spacing for the FFT grid is 0.1 nm, and fourth-order interpolation is used. Because periodic boundary conditions are required for the Ewald summation, the ice nanocrystals were placed in supercells, ensuring that there was at least 5 nm of vacuum around the crystals. For the 768 water molecule crystal, all interactions were calculated in real space.

A series of MD simulations from 30 K up to the melting point were performed for each cluster. Long NVT runs were performed, and especially when the temperature approached the melting point, the MD simulations were run for at least 45 ns. It can be seen from Figure 6 that for certain temperatures (near the melting point) such long simulations were essential. Analysis was performed on the last 15 ns of each simulation, with data sampled every 0.5 to 2.5 ps on at least 2400 independent configurations.

The ice Ih crystals used in this study require some comment. Although the habit diagram of ice crystals shows a rich variety of structures, to the best of our knowledge the equilibrium crystal shape of ice crystals has not been determined.[57] Given that the basal and prism faces of ice have similar surface energies[58] and that hexagonal platelets are a commonly observed morphology, we opted for a range of hexagonal nanocrystals with similar areas of basal and prism face exposed, and hence the aspect ratio of the crystals is approximately constant (see Figure 1). Nanocrystals with 9600, 6144, 2592, and 768 water molecules were examined, and they all had disordered proton arrangements in the bulk but ordered proton arrangements at the surfaces, to be consistent with recent studies on the ice basal[59,60] and prism[58] surfaces, which showed that at these surfaces protons prefer ordered arrangements. To generate proton disordered arrangements in the bulk, we used Rahman and Stillinger's algorithm,[61,62] which we find to be very efficient for the large systems considered here. Naturally occurring ice crystals are unlikely to be as perfect and defect-free as the nanocrystals modeled here and, in particular, may have significant amorphous character. Although it would be interesting to explore how such clusters melt, this is something that is beyond the scope of the present study.

Acknowledgment. D.P. and E.G.W. are supported by NSFC. D.P. is grateful to the Thomas Young Centre for a Junior Research Fellowship. A.M. is supported by the EURYI scheme, the EPSRC, and the European Research Council. Computational resources from the London Centre for Nanotechnology and UCL Research Computing are warmly acknowledged. Also *via* our membership to the UK's HPC Materials Chemistry Consortium, which is funded by EPSRC (EP/F067496), this work made use of the facilities of HECToR, the UK's national high-performance computing service.

REFERENCES AND NOTES

1. Faraday, M. *Faraday's Diary*, Vol. IV; Bell and Sons: London, 1933.
2. Bluhm, H.; Salmeron, M. Growth of Nanometer Thin Ice Films from Water Vapor Studied Using Scanning Polarization Force Microscopy. *J. Chem. Phys.* **1999**, *111*, 6947.
3. Bluhm, H.; Inoue, T.; Salmeron, M. Friction of Ice Measured Using Lateral Force Microscopy. *Phys. Rev. B* **2000**, *61*, 7760–7765.
4. Bluhm, H.; Ogletree, D. F.; Fadley, C. S.; Hussain, Z.; Salmeron, M. The Premelting of Ice Studied with Photoelectron Spectroscopy. *J. Phys.: Condens. Matter* **2002**, *14*, L227.
5. Lied, A.; Dosch, H.; Bilgram, J. H. Surface Melting of Ice I(h) Single Crystals Revealed by Glancing Angle X-Ray Scattering. *Phys. Rev. Lett.* **1994**, *72*, 3554–3557.
6. Dosch, H.; Lied, A.; Bilgram, J. H. Glancing-Angle X-Ray Scattering Studies of the Premelting of Ice Surfaces. *Surf. Sci.* **1995**, *327*, 145–164.
7. Dosch, H.; Lied, A.; Bilgram, J. H. Disruption of the Hydrogen-Bonding Network at the Surface of Ih Ice Near Surface Premelting. *Surf. Sci.* **1996**, *366*, 43–50.
8. Li, Y.; Somorjai, G. A. Surface Premelting of Ice. *J. Phys. Chem. C* **2007**, *111*, 9631–9637.
9. Materer, N.; Starke, U.; Barbieri, A.; Van Hove, M.; Somorjai, G. A.; Kroes, G. J.; Minot, C. Molecular Surface Structure of a Low-Temperature Ice Ih (0001) Crystal. *J. Phys. Chem.* **1995**, *99*, 6267–6269.
10. Sadtchenko, V.; Ewing, G. E. A New Approach to the Study of Interfacial Melting of Ice: Infrared Spectroscopy. *Can. J. Phys.* **2003**, *81*, 333–341.
11. Kroes, G. J. Surface Melting of the (0001) Face of TIP4P Ice. *Surf. Sci.* **1992**, *275*, 365–382.
12. Furukawa, Y.; Nada, H. Anisotropic Surface Melting of an Ice Crystal and its Relationship to Growth Forms. *J. Phys. Chem. B* **1997**, *101*, 6167–6170.
13. Nada, H.; Furukawa, Y. Anisotropy in Structural Phase Transitions at Ice Surfaces: a Molecular Dynamics Study. *Appl. Surf. Sci.* **1997**, *121*, 445–447.
14. Carignano, M. A.; Shepson, P. B.; Szleifer, I. Molecular Dynamics Simulations of Ice Growth from Supercooled Water. *Mol. Phys.* **2005**, *103*, 2957–2967.
15. Ikeda-Fukazawa, T.; Kawamura, K. Molecular-Dynamics Studies of Surface of Ice Ih. *J. Chem. Phys.* **2004**, *120*, 1395.
16. Paesani, F.; Iuchi, S.; Voth, G. A. Quantum Effects in Liquid Water from an Ab Initio-Based Polarizable Force Field. *J. Chem. Phys.* **2007**, *127*, 074506.

17. Conde, M. M.; Vega, C.; Patrykiejew, A. The Thickness of a Liquid Layer on the Free Surface of Ice as Obtained from Computer Simulation. *J. Chem. Phys.* **2008**, *129*, 014702.
18. Bishop, C. L.; Pan, D.; Liu, L. M.; Tribello, G. A.; Michaelides, A.; Wang, E. G.; Slater, B. On Thin Ice: Surface Order and Disorder during Pre-Melting. *Faraday Discuss.* **2009**, *141*, 277–292.
19. Delzeit, L.; Blake, D. A Characterization of Crystalline Ice Nanoclusters Using Transmission Electron Microscopy. *J. Geophys. Res.* **2001**, *106*, 33371–33379.
20. Murray, B. J.; Jensen, E. J. Homogeneous Nucleation of Amorphous Solid Water Particles in the Upper Mesosphere. *J. Atmos. Sol.-Terr. Phys.* **2010**, *72*, 51–61.
21. Hock, C.; Schmidt, M.; Kuhnen, R.; Bartels, C.; Ma, L.; Haberland, H.; v. Issendorff, B. Calorimetric Observation of the Melting of Free Water Nanoparticles at Cryogenic Temperatures. *Phys. Rev. Lett.* **2009**, *103*, 73401.
22. Mitsui, T.; Rose, M. K.; Fomin, E.; Ogletree, D. F.; Salmeron, M. Water Diffusion and Clustering on Pd (111). *Science* **2002**, *297*, 1850.
23. Michaelides, A.; Morgenstern, K. Ice Nanoclusters at Hydrophobic Metal Surfaces. *Nat. Mater.* **2007**, *6*, 597–601.
24. Mehlhorn, M.; Carrasco, J.; Michaelides, A.; Morgenstern, K. Local Investigation of Femtosecond Laser Induced Dynamics of Water Nanoclusters on Cu (111). *Phys. Rev. Lett.* **2009**, *103*, 26101.
25. Egorov, A. V.; Brodskaya, E. N.; Laaksonen, A. Solid-Liquid Phase Transition in Small Water Clusters: a Molecular Dynamics Simulation Study. *Mol. Phys.* **2002**, *100*, 941–951.
26. Pereyra, R. G.; Carignano, M. A. Ice Nanocolumns: a Molecular Dynamics Study. *J. Phys. Chem. C* **2009**, *113*, 12699–12705.
27. Huang, J.; Bartell, L. S. Kinetics of Homogeneous Nucleation in the Freezing of Large Water Clusters. *J. Phys. Chem.* **1995**, *99*, 3924–3931.
28. Tiller, W. A. *The Science of Crystallization: Microscopic Interfacial Phenomena*; Cambridge University Press: Cambridge, 1991.
29. Makkonen, L. On The Methods to Determine Surface Energies. *Langmuir* **2000**, *16*, 7669–7672.
30. Makkonen, L. The Gibbs-Thomson Equation and the Solid-Liquid Interface. *Langmuir* **2002**, *18*, 1445.
31. Della Volpe, C.; Siboni, S.; Morra, M. Comments on Some Recent Papers on Interfacial Tension and Contact Angles. *Langmuir* **2002**, *18*, 1441–1444.
32. Campbell, C. T.; Parker, S. C.; Starr, D. E. The Effect of Size-Dependent Nanoparticle Energetics on Catalyst Sintering. *Science* **2002**, *298*, 811.
33. In eq 1, the TIP4P bulk ice melting temperature $T_m^b = 230 \pm 3$ K is used.[17] L is 2.29×10^{11} mJ/m^3.[66] As for the curvature, $K = 2/R$ for a sphere is used since at the melting point the clusters are almost spherical. R is the average radius of each of the melted spherical-like water clusters. The only uncertain parameter in eq 1 is the ice/water surface energy γ. In Figure 4 the fitted ice/water surface energy is 46.7 mJ/m^2 (2.92 meV/Å^2). This is somewhat larger than the values reported in refs 63 and 64 of 29 mJ/m^2 and in ref 65 of 31.7 ± 2.7 mJ/m^2. However, our fitted value is of the same order of magnitude, and given the complicated nature of the ice/water interface, with, for example, the premelting involved, this seems acceptable.
34. It is worth noting that the Gibbs–Thomson equation is just a first-order theory. Mori *et al.* have given a second-order expansion[64] (also discussed by Makkonen[30]). However, the second-order correction is relevant to only extremely small ice clusters. For example, the error estimated is only 2 K for a sphere of $r = 2$ nm.[64] Such a small difference between the first- and second-order theories can easily be concealed in the fluctuations in the MD simulations for the clusters considered here.
35. Farrell, H. H.; Van Siclen, C. D. Binding Energy, Vapor Pressure, and Melting Point of Semiconductor Nanoparticles. *J. Vac. Sci. Technol. B* **2007**, *25*, 1441–1447.
36. Baker, M. B.; Dash, J. G. Charge Transfer in Thunderstorms and the Surface Melting of Ice. *J. Cryst. Growth* **1989**, *97*, 770.
37. Nenow, D.; Trayanov, A. Surface Melting of Small Crystals. *J. Cryst. Growth* **1990**, *99*, 102.
38. The data points for premelting thickness *versus* temperature are fitted to the empirical relation[57] $d(T) = \lambda \ln(c(T_m^c)/(T_m^c - T)$, so when $d(T) = 0.1$ nm, we can get the premelting temperature T_{pm}^c.
39. The water molecules in the topmost surface layer of the ice crystals are not considered as quasi-liquid molecules at low temperatures. The difference between the premelting layer thicknesses on the basal and prism surfaces is consistent with the "apparent" values reported in Conde *et al.*[17]
40. Plane, J.; Murray, B. J.; Chu, X.; Gardner, C. S. Removal of Meteoric Iron on Polar Mesospheric Clouds. *Science* **2004**, *304*, 426–428.
41. Murray, B. J.; Plane, J. M. C. Uptake of Fe, Na and K Atoms on Low-Temperature Ice: Implications for Metal Atom Scavenging in the Vicinity of Polar Mesospheric Clouds. *Phys. Chem. Chem. Phys.* **2005**, *7*, 3970–3979.
42. Perdew, J. P.; Burke, S.; Ernzerhof, M. Generalized Gradient Approximation Made Simple. *Phys. Rev. Lett.* **1996**, *77*, 3865.
43. Becke, A. D. Density-Functional Exchange-Energy Approximation with Correct Asymptotic Behavior. *Phys. Rev. A* **1988**, *38*, 3098.
44. Lee, C.; Yang, W.; Parr, R. C. Development of the Colle-Salvetti Correlation-Energy Formula into a Functional of the Electron Density. *Phys. Rev. B* **1988**, *37*, 785.
45. Sprik, M.; Hutter, J.; Parrinello, M. Ab Initio Molecular Dynamics Simulation of Liquid Water: Comparison of three Gradient-Corrected Density Functionals. *J. Chem. Phys.* **1996**, *105*, 1142.
46. Yoo, S.; Zeng, X. C.; Xantheas, S. S. On the Phase Diagram of Water with Density Functional Theory Potentials: the Melting Temperature of Ice I with the Perdew–Burke–Ernzerhof and Becke–Lee–Yang–Parr Functionals. *J. Chem. Phys.* **2009**, *130*, 221102.
47. Jorgensen, W. L.; Chandrasekhar, J.; Madura, J. D.; Impey, R. W.; Klein, M. L. Comparison of Simple Potential Functions for Simulating Liquid Water. *J. Chem. Phys.* **1983**, *79*, 926.
48. Sanz, E.; Vega, C.; Abascal, J. L. F.; MacDowell, L. G. Phase Diagram of Water from Computer Simulation. *Phys. Rev. Lett.* **2004**, *92*, 255701.
49. Karim, O. A.; Haymet, A. D. J. The Ice/Water Interface: a Molecular Dynamics Simulation Study. *J. Chem. Phys.* **1988**, *89*, 6889.
50. Abascal, J. L. F.; Sanz, E.; Fernández, R. G.; Vega, C. A Potential Model for the Study of Ices and Amorphous Water: TIP4P/Ice. *J. Chem. Phys.* **2005**, *122*, 234511.
51. Abascal, J. L. F.; Vega, C. A General Purpose Model for the Condensed Phases of Water: TIP4P/2005. *J. Chem. Phys.* **2005**, *123*, 234505.
52. Berendsen, H. J. C.; Grigera, J. R.; Straatsma, T. P. The Missing Term in Effective Pair Potentials. *J. Chem. Phys.* **1987**, *91*, 6269.
53. Van Der Spoel, D.; Lindahl, E.; Hess, B.; Groenhof, G.; Mark, A. E.; Berendsen, H. J. C. GROMACS: Fast, Flexible, and Free. *J. Comput. Chem.* **2005**, *26*, 1701.
54. Nosé, S. A Molecular Dynamics Method for Simulations in the Canonical Ensemble. *Mol. Phys.* **1984**, *52*, 255–268.
55. Hoover, W. G. Canonical Dynamics: Equilibrium Phase-Space Distributions. *Phys. Rev. A* **1985**, *31*, 1695.
56. Essmann, U.; Perera, L.; Berkowitz, M. L.; Darden, T.; Lee, H.; Pedersen, L. G. A. Smooth Particle Mesh Ewald Method. *J. Chem. Phys.* **1995**, *103*, 8577–8593.
57. Libbrecht, K. G. The Physics of Snow Crystals. *Rep. Prog. Phys.* **2005**, *68*, 855–895.
58. Pan, D.; Liu, L. M.; Tribello, G. A.; Slater, B.; Michaelides, A.; Wang, E. Surface Energy and Surface Proton Order of the Ice Ih Basal and Prism Surfaces. *J. Phys.: Condens. Matter* **2010**, *22*, 074209.
59. Pan, D.; Liu, L. M.; Tribello, G. A.; Slater, B.; Michaelides, A.; Wang, E. Surface Energy and Surface Proton Order of Ice Ih. *Phys. Rev. Lett.* **2008**, *101*, 155703.

60. Buch, V.; Groenzin, H.; Li, I.; Shultz, M. J.; Tosatti, E. Proton Order in the Ice Crystal Surface. *Proc. Natl. Acad. Sci. U. S. A.* **2008**, *105*, 5969.
61. Rahman, A.; Stillinger, F. H. Proton Distribution in Ice and the Kirkwood Correlation Factor. *J. Chem. Phys.* **1972**, *57*, 4009.
62. In order to prepare the hexagonal ice nanocrystals, orthorhombic supercells were built by replicating ice unit cells by translation *nx*, *ny*, *nz* times in the *x*, *y*, *z* directions. 9600 waters: 15 × 10 × 8; 6144 waters: 12 × 8 × 8; 2592 waters: 9 × 6 × 6; 768 waters: 6 × 4 × 4. The size of the initial replicated unit cell is 4.44, 7.70, and 7.26 Å in *x*, *y*, and *z* directions. In order to produce regular hexagonal shapes, the ratio between the translation vectors was kept at *nx*:*ny* = 3:2. Once the orthorhombic supercell has been built, the two corners of the cell are moved to the opposite sides of the crystal to make an ice cluster with hexagonal platelet structure. With zero dipole moment for the initial orthorhombic supercell, Rahman and Stillinger's algorithm can ensure that the dipole moment of the generated structure remains zero.[61] All the ice nanoclusters examined here have proton disordered interiors and proton ordered surfaces.
63. Makkonen, L. Surface Melting of Ice. *J. Phys. Chem. B* **1997**, *101*, 6196–6200.
64. Mori, A.; Maruyama, M.; Furukawa, Y. Second-Order Expansion of Gibbs-Thomson Equation and Melting Point Depression of Ice Crystallite. *J. Phys. Soc. Jpn.* **1996**, *65*, 2742–2744.
65. Hillig, W. B. Measurement of Interfacial Free Energy for Ice/Water System. *J. Cryst. Growth* **1998**, *183*, 463–468.
66. Vega, C.; Abascal, J. L. F.; Conde, M. M.; Aragones, J. L. What Ice Can Teach Us about Water Interactions: A Critical Comparison of the Performance of Different Water Models. *Faraday Discuss.* **2009**, *141*, 251–276.